Photodissociation of the HeH^+ ion into excited fragments ($n=2,3$) by time-dependent methods

K. Sodoga,[1,2] J. Loreau,[3] D. Lauvergnat,[1] Y. Justum,[1] N. Vaeck,[3] and M. Desouter-Lecomte[1,4,*]
[1]*Laboratoire de Chimie Physique, Université de Paris-Sud, UMR 8000, Bât 349, Orsay F-91405, France*
[2]*Université de Lomé, Faculté des Sciences, Département de Physique, BP 1515 Lomé, Togo*
[3]*Laboratoire de Chimie Quantique et Photophysique, Université Libre de Bruxelles, CP160/09 50, av. F. Roosevelt, 1050 Bruxelles, Belgium*
[4]*Département de Chimie, B6c, Université de Liège, Sart-Tilman, B-4000 Liège 1, Belgium*
(Received 12 June 2009; published 28 September 2009)

The total and partial photodissociation cross sections of the molecular ion HeH^+ are computed by time-dependent methods for fragmentation into the excited shells $n=1,2,3$ up to a photon energy of 40 eV. $^1\Sigma^+$ and $^1\Pi$ states are considered for parallel and perpendicular transitions for different initial rotational or vibrational excitations. Nonadiabatic radial and rotational couplings are taken into account. The results from coupled-channel equations are compared with the Born-Oppenheimer approximation. A time-dependent calculation with a femtosecond laser pulse is carried out to simulate a recent crossed beam photodissociation imaging experiment with vacuum ultraviolet free-electron laser [H. B. Pedersen *et al.*, Phys. Rev. Lett. **98**, 223202 (2007)]. The dominance of photodissociation perpendicular to the photon polarization is confirmed.

DOI: 10.1103/PhysRevA.80.033417 PACS number(s): 33.80.−b, 34.70.+e

I. INTRODUCTION

The HeH^+ helium-hydride molecular ion has been the subject of numerous experimental [1–6] and theoretical works [7–16] due to its interest in the context of astrophysics [17–19]. It has been suggested that HeH^+ could be abundant enough in different celestial objects composed of primordial material such as metal-poor stars, white dwarfs or the planetary nebula, to be observed in the infrared domain [20]. However, despite numerous efforts, none of the several attempts of extraterrestrial observation of HeH^+ have been conclusive. One of the key points in the evaluation of the fractional abundance of HeH^+ is to determine a correct balance between the formation and destruction rate processes; one of these processes being photodissociation. The rate of photodissociation was determined either by detailed balancing applied to the reverse reaction, i.e. radiative association [19,21] or by absorption from the ground state to the vibrational continuum of the first excited state only [17,22]. Recently, the first experimental data on the photodissociation of HeH^+, i.e., a crossed beam photodissociation imaging with vacuum ultra violet free-electron laser in Hamburg FLASH [23] has renewed the interest in the fragmentation into highly excited fragments ($n\geq 2$). The experiment involves photons of wavelength 32 nm (38.7 eV) and resolves the kinetic energy release of the neutral He fragment and the corresponding angular distribution with respect to the photon polarization. This experiment on the HeH^+ system reveals the dominance of photodissociation perpendicular to the laser polarization and therefore the important role of the Π states during dissociation with energetic photons. This shows the necessity of taking into account the perpendicular orientation generally not considered or not completely considered in previous theoretical models. The photodissociation has been recently revisited for both orientations [16] and compared with previous results for parallel orientation [12]. The cross section is computed in Ref. [16] by the Fermi Golden rule within the Born-Oppenheimer approximation with a possible correction to consider the avoided crossing between the second and third excited states of the Σ manifold. In this work, we present a time-dependent approach of the photodissociation by including all the radial nonadiabatic couplings and the rotational couplings between the $^1\Sigma$ and $^1\Pi$ states. The time-dependent approach is equivalent to the Golden rule treatment [24]. In a first approach, the total photodissociation cross section is computed using the autocorrelation function of the promoted state by considering different vibrational and rotational initial states and the partial cross section is obtained by two different methods using the asymptotic wave packets. Secondly, we simulate the free-electron laser experiment by exciting the ground initial state with a Gaussian laser pulse of 30 fs and a carrier frequency corresponding to the experimental wavelength. The kinetic energy of the He fragment is estimated from the asymptotic wave packets in order to compare with the experimental data.

II. COMPUTATIONAL DETAILS

A. Molecular data

We consider the singlet $^1\Sigma^+$ and the $^1\Pi$ adiabatic electronic states which dissociate into $He(1snl)+H^+$ and $He^+(1s)+H(nl)$ with $n=1,2,3$. There exist 12 e-labeled $^1\Sigma^+$ states, 6 e-labeled $^1\Pi^e$ and 6 f-labeled $^1\Pi^f$. The parity under the E^* inversion operator in the laboratory frame [25] of a ro-electronic state is given by $(-1)^J\varepsilon$, where J is the quantum number of the rotation and $\varepsilon=+1$ or -1 correspond to e or f states [26]. For the electronic part, the E^* inversion corresponds to the reflection in the xz plane of the molecular frame. Due to symmetry, there is no nonadiabatic coupling between the e and f states [27]. The potential energy curves and couplings are computed at the state average complete active space self-consistent field (CASSCF) [28] level by

*Corresponding author; mdesoute@lcp.u-psud.fr

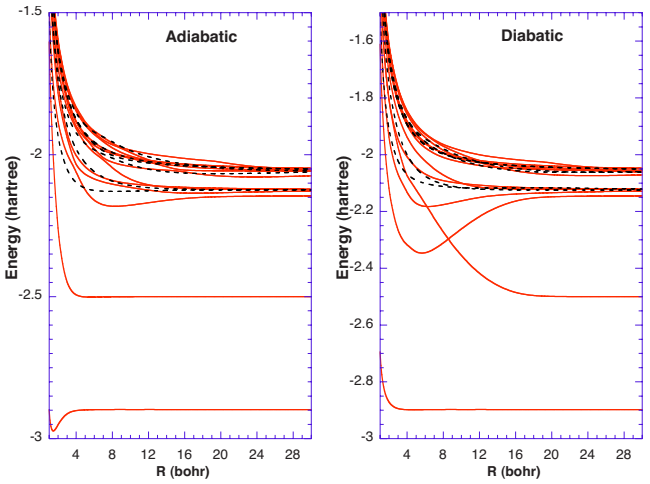

FIG. 1. (Color online) Adiabatic and diabatic potential energy curves of the $^1\Sigma^+$ (full lines) and $^1\Pi$ (dashed lines) of the HeH^+ molecular ion. The adiabatic curves are computed at the state average CASSCF level. The diabatic curves are obtained from the transformation matrix $\mathbf{D}(R)$ solution of the equation $\partial_R\mathbf{D}(R)=-\mathbf{F}(R)\mathbf{D}(\mathbf{R})$ where $\mathbf{F}(R)$ is the approximate "2×2" nonadiabatic radial coupling matrix.

using the *ab initio* quantum chemistry package MOLPRO [29]. A large nonstandard basis set is used by adding one contracted Gaussian per orbital per atom up to $n=4$ to the aug-cc-pV5Z basis set (augmented correlation-consistent valence quintuple zeta) [30]. Details and comparison with other theoretical works are given in Ref. [31]. The CASSCF approach allows the computation of the radial nonadiabatic coupling elements of the first derivative ∂_R operator. The $\mathbf{F}(R)$ matrix $F_{\alpha\beta}(R)=\langle\chi_\alpha^{ad}|\partial_R|\chi_\beta^{ad}\rangle$ is used to build diabatic electronic states by solving the coupled equations $\partial_R\mathbf{D}(R)=-\mathbf{F}(R)\mathbf{D}(\mathbf{R})$ for the elements of the adiabatic-to-diabatic $\mathbf{D}(R)$ matrix transformation

$$\mathbf{V}^{dia}(R)=\mathbf{D}^T(R)\mathbf{V}^{adia}(R)\mathbf{D}(R),$$

where $\mathbf{V}$ is the matrix of the electronic Hamiltonian $\hat{H}_{el}$ which is diagonal in the adiabatic representation. We use an approximate $\mathbf{F}(R)$ matrix by retaining only the main couplings between neighboring states. This structure corresponds to a succession of 2×2 coupling cases. This approach, which reduces considerably the computational cost and simplifies the diabatization procedure, has been shown to give similar results to the use of the complete $\mathbf{F}(R)$ matrix in curve crossing dynamics [32]. The adiabatic and diabatic potential energy curves are represented in Fig. 1. The dissociation channels for the $^1\Sigma^+$ and $^1\Pi$ states are gathered in Table I. The Stark effect due to He^+ lifts the degeneracy of the excited hydrogen atom as it has been already mentioned in Ref. [8].

We also include in the time-dependent treatment the effect of the rotational couplings but we neglect the spin-dependent interactions. The field free Hamiltonian is $\hat{H}_0=\hat{H}_{el}+\hat{T}_{rad}+\hat{T}_{rot}$. We use a basis set of electronic-rotational functions to get time-dependent coupled equations for the nuclear motion. These parity adapted functions are

$$|mJM\Lambda\varepsilon\rangle=\frac{1}{[2(1+\delta_{\Lambda0})]^{1/2}}[|JM\Lambda\rangle|m\Lambda\rangle+(-1)^J\varepsilon|JM,-\Lambda\rangle|m(-\Lambda)\rangle]$$

where m numbers the electronic states for a given Λ.

TABLE I. CASSCF asymptotic energies of the $^1\Sigma^+$ and $^1\Pi$ states included in the calculations.

State m	Energy (h) at 50 bohr	Dissociative atomic states
1	−2.8980458	Σ, $He(1s^2\ ^1S)+H^+$
2	−2.4999359	Σ, $He^+(1s)+H(1s)$
3	−2.1448183	Σ, $He(1s2s\ ^1S)+H^+$
4	−2.1261793	Σ, $He^+(1s)+1/\sqrt{2}[H(2s)-H(2p)]$
5	−2.1237656	Σ, $He^+(1s)+1/\sqrt{2}[H(2s)+H(2p)]$
6	−2.1225613	Σ, $He(1s2p\ ^1P^o)+H^+$
7	−2.0623295	Σ, $He(1s3s\ ^1S)+H^+$
8	−2.0600078	Σ, $He^+(1s)+1/\sqrt{3}\cdot H(3s)+1/\sqrt{2}\cdot H(3p)+1/\sqrt{6}\cdot H(3d)$
9	−2.0568303	Σ, $He(1s3d\ ^1D)+H^+$
10	−2.0552158	Σ, $He^+(1s)+1/\sqrt{3}.H(3s)-\sqrt{2/3}.H(3d)$
11	−2.0528106	Σ, $He(1s3p\ ^1P^o)+H^+$
12	−2.0523058	Σ, $He^+(1s)+1/\sqrt{3}\cdot H(3s)-1/\sqrt{2}\cdot H(3p)+1/\sqrt{6}\cdot H(3d)$
1	−2.1248933	Π, $He^+(1s)+H(2p)$
2	−2.1236547	Π, $He(1s2p\ ^1P^o)+H^+$
3	−2.0571436	Π, $He^+(1s)+1/\sqrt{2}[H(3p)-H(3d)]$
4	−2.0567818	Π, $He(1s3d\ ^1D)+H^+$
5	−2.0536464	Π, $He^+(1s)+1/\sqrt{2}[H(3p)+H(3d)]$
6	−2.0531961	Π, $He(1s3p\ ^1P^o)+H^+$

$|JM\Lambda\rangle=[(2J+1)/4\pi]^{1/2}D^{(J)*}_{M\Lambda}(\phi,\theta,0)$ are the eigenstates of the total angular momentum representation where D is a Wigner function [27]. M and Λ are the projection of the total electronic angular momentum L onto the laboratory Z axis and onto the internuclear z axis, respectively. Λ is also the projection of the total molecular angular momentum J onto the internuclear axis because in this case the total electronic spin S is zero ($\Omega=\Lambda+S=\Lambda$). The rotational kinetic operator takes the form $\hat{T}_{rot}=\hat{N}^2/(2\mu R^2)$ with $\hat{N}^2=\hat{J}^2+\hat{L}^2-2\hat{J}.\hat{L}$ and $\hat{J}.\hat{L}=\hat{J}_z\hat{L}_z+(\hat{J}_+\hat{L}_-+\hat{J}_-\hat{L}_+)/2$. After the action of the ladder operator $\hat{J}_\pm|JM\Lambda\rangle=[J(J+1)-\Lambda(\Lambda\mp1)]^{1/2}|JM,\Lambda\mp1\rangle$, the rotational couplings between symmetry adapted $\Sigma(\Lambda=0)$ and $\Pi(\Lambda=\pm1)$ states become

$$\langle m'J'M'\Sigma|\hat{T}_{rot}|mJM\Pi^e\rangle = -\frac{[J(J+1)]^{1/2}}{2\mu R^2}\frac{1}{2^{1/2}}(\langle m'\Sigma|\hat{L}_-|m\Lambda=1\rangle + \langle m'\Sigma|\hat{L}_+|m\Lambda=-1\rangle)\delta_{J,J'}\delta_{MM'}.$$

For diatomic molecules, MOLPRO works in the C_{2v} group, which allows us to calculate the matrix elements of L_x and L_y between the Σ states and the Π_x and Π_y components of the Π states. We obtain the matrix elements $\langle m'\Sigma|\hat{L}_y|m\Pi_x\rangle=-ia_{m'm}$ and $\langle m'\Sigma|\hat{L}_x|m\Pi_y\rangle=ia_{m'm}$, and transform them in order to get $\langle m'\Sigma|\hat{L}_\pm|m\Lambda=\mp1\rangle$. The final expression of the rotational couplings is

$$\langle m'J'M'\Sigma|\hat{T}_{rot}|mJM\Pi\rangle=[J(J+1)]^{1/2}a_{m'm}/(\mu R^2)\delta_{J,J'}\delta_{MM'}.$$

We neglect the contribution from the $(\hat{L}_x^2+\hat{L}_y^2)/2\mu R^2$ term. In the diagonal rotational correction ($m=m'$ and $\Lambda=\Lambda'$), we include the term

$$\langle m'J'M'\Lambda'|\hat{T}_{rot}|mJM\Lambda\rangle = [J(J+1)-2\Lambda^2]/(2\mu R^2)\delta_{mm'}\delta_{\Lambda\Lambda'}\delta_{J,J'}\delta_{MM'}.$$

The rotational coupling matrix is computed in the adiabatic basis set and transformed to the diabatic one

$$\mathbf{T}^{dia}_{rot}(R)=\mathbf{D}^T(R)\mathbf{T}^{adia}_{rot}(R)\mathbf{D}(R).$$

B. Photodissociation cross section

The photodissociation cross section towards $^1\Sigma$ or $^1\Pi$ states from a ro-vibrational state $\chi^{adia}_{0v''J''}(R)$ of energy $E_{0v''J''}$ where 0 denotes the ground electronic state $^1\Sigma^+(\Lambda''=0)$ is

$$\sigma_{0v''J''\to\Lambda'}(E)=\sum_{J'}\frac{S_{J''\Lambda'',J'\Lambda'}}{2J'+1}\sigma_{0v''J''\to\Lambda'J'}(E), \quad (1)$$

where the Hönl-London factor for symmetry adapted states is given by [33]

$$S_{J''\Lambda'',J'\Lambda'}=(1+\delta_{\Lambda'0}+\delta_{\Lambda''0}-2\delta_{\Lambda'0}\delta_{\Lambda''0})(2J'+1)\times(2J''+1)\begin{pmatrix}J' & 1 & J''\\ -\Lambda' & \Lambda'-\Lambda'' & \Lambda''\end{pmatrix}^2.$$

Each contribution $\sigma_{0v''J''\to\Lambda'J'}(E)$ is obtained by Fourier transforming the autocorrelation function $C^{0v''J''}_{\Lambda'J'}(t)=\Sigma_m\langle\Phi^{0v''J''}_{m\Lambda'J'}(t=0)|\Phi^{0v''J''}_{m\Lambda'J'}(t)\rangle$ of a promoted state $\mathbf{\Phi}^{0v''J''}_{m\Lambda'J'}(t=0)$. In the adiabatic representation, each component $\Phi^{0v''J''ad}_{m\Lambda'J'}(t=0)=\mu^{ad}_{j,0\to m\Lambda'}(R)\chi^{ad}_{0v''J''}(R)$ is built by multiplying the initial nuclear state $\chi^{ad}_{0v''J''}(R)$ of the ground adiabatic electronic state by the adiabatic components of the transition moment $\mu^{ad}_{j,0\to m\Lambda'}$, with $j=x,y,z$. The vector is then transformed to the diabatic representation $\mathbf{\Phi}^{dia}(t=0)=\mathbf{D}(R)\mathbf{\Phi}^{adia}(t=0)$ and propagated with the field free coupled equations on the excited states with angular momentum J' with $J'=J''-1$ and $J''+1$ for the $^1\Sigma\to{}^1\Sigma$ transitions and $J'=J''-1$ and $J''+1$ (involving $^1\Pi^e$ states) and $J'=J''$ (involving $^1\Pi^f$ states) for $^1\Sigma\to{}^1\Pi$ transitions ($J'=1$ only when $J''=0$). The cross section $\sigma_{0v''J''\to\Lambda'J'}(E)$ in SI units is then given by [34,35]

$$\sigma_{0v''J''\to\Lambda'J'}(E)=4\pi^2\alpha a_0^2EA^{0v''J''}_{\Lambda'J'}(E), \quad (2)$$

where $\alpha=e^2/(\hbar c4\pi\varepsilon_0)$ is the fine structure constant and a_0 is the Bohr radius and

$$A^{0v''J''}_{\Lambda'J'}(E)=2\mathrm{Re}\left[\frac{1}{2\pi}\int_0^\infty C^{0v''J''}_{\Lambda'J'}(t)e^{i(E_{0v''J''}+E)t/\hbar}dt\right]$$

The partial cross sections can be obtained by different methods from an analysis of the wave packets in the asymptotic region. The first one uses the Fourier transformation of each component of the wave packet at a large internuclear distance, R_∞, where the couplings become vanishingly small and the dissociation channels are diabatic or adiabatic [36]. Then the partial cross-section is given by

$$\sigma_{0v''J''\to m\Lambda'J'}(E)=\frac{4\pi^2\alpha a_0^2k_m}{\mu}E|A^{0v''J''}_{m\Lambda'J'}(E)|^2, \quad (3)$$

where $k_m=\sqrt{2\mu(E-E^{as}_m)}/\hbar$ is the magnitude of the wave number in dissociative channel m with an asymptotic energy E^{as}_m and

$$A^{0v''J''}_{m\Lambda'J'}(E)=\frac{1}{\sqrt{2\pi}}\int_0^\infty\Phi^{0v''J''}_{m\Lambda'J'}(R_\infty,t)e^{i(E_{0v''J''}+E)t/\hbar}dt.$$

The second method uses the momentum representation of the wave packet [37,35]

$$\bar{\Phi}^{0v''J''}_{m\Lambda'J'}(k,t_\infty)=\frac{1}{\sqrt{2\pi}}\int_0^\infty\Phi^{0v''J''}_{m\Lambda'J'}(R,t_\infty)e^{-ikR}dR$$

and leads to the expression

$$\sigma_{0v''J''\to m\Lambda'J'}(E)=\frac{4\pi^2\alpha a_0^2\mu}{k_n}E|\bar{\Phi}^{0v''J''}_{m\Lambda'J'}(k,t_\infty)|^2. \quad (4)$$

The field free propagation is carried out in diabatic representation by the split operator method [38] extended to nonadia-

batic processes formalism [39]. This requires two transformations to change from the diabatic to the rotationally adiabatic representation (by diagonalizing the J' bloc of the matrix of $\hat{H}_{el}+\hat{T}_{rot}$) and two Fourier transformations to change from the coordinate to the momentum representations in order to apply the kinetic part of the propagator. The method based on Eq. (4) requires a larger spatial grid than the approach based on Eq. (3) since at the final time, the whole wave packet must be in the asymptotic region before the optical potential which avoids the reflection at the end of the grid. We use 2^{13} points for a grid of 100 a.u. A quadratic optical potential begins at 80 a.u. The asymptotic point R_∞ [Eq. (3)] is 35 a.u. and the final time t_∞ [Eq. (4)] is 61 fs. The time step is 2.41×10^{-2} fs.

C. Dynamics with a femtosecond pulse

The propagation is carried out again by the split operator by keeping the field constant during a small time interval. The elementary evolution operator for a time step is given by

$$U(\Delta t)\psi(t_k) = e^{-i\Delta t/(4\hbar)\mathbf{V}}e^{i\Delta t/(2\hbar)\boldsymbol{\mu}\varepsilon(t_k)}e^{-i\Delta t/(4\hbar)\mathbf{V}}e^{-i\Delta t/\hbar\mathbf{T}} \times e^{-i\Delta t/(4\hbar)\mathbf{V}}e^{i\Delta t/(2\hbar)\boldsymbol{\mu}\varepsilon(t_k)}e^{-i\Delta t/(4\hbar)\mathbf{V}}\psi(t_k).$$

The propagator $e^{i\Delta t/(2\hbar)\boldsymbol{\mu}\varepsilon(t_k)}$ is built by diagonalizing the transition moment matrix $\boldsymbol{\mu}$ one time and by multiplying at each step the eigenvalues by the scalar $\varepsilon(t_k)$.

We use a Gaussian femtosecond laser field with parameters inspired from the experimental conditions. The carrier frequency is fixed by the experimental wave length (32 nm). The half-height width of the envelope is 30 fs. The total duration of the propagation is 100 fs with a time step of 2.41×10^{-2} fs. We use an intensity of 8.775×10^{11} W cm^{-2} which is larger than the experimental intensity but the probabilities of transition

$$P_m(t) = \langle \Phi^{0v''J''}_{m\Lambda'J'}(t) | \Phi^{0v''J''}_{m\Lambda'J'}(t) \rangle \quad (5)$$

are very weak and we increased the intensity in order to obtain probabilities of the order of 0.1%.

III. PHOTODISSOCIATION CROSS SECTION

Figure 2 shows the photodissociation cross section $\sigma_{0v''J''\to\Lambda'}(E)$ computed by Eqs. (1) and (2) for $^1\Sigma\to{}^1\Sigma$, i.e. for the parallel orientation of the molecular axis with respect to the field for different initial states. The cases $J''=0\to J'=1$ (full line) and $J''=1\to J'=0,2$ (dotted line with open circles) for $v=0$ are nearly superimposed showing a negligible influence of the rotational excitation (the difference between the maximum of the cross section for $J'=0$ and $J'=2$ is 0.07%). We also show two cases with higher rotational and with vibrational excitation. The example $J''=10\to J'=9,11$ for $v=0$ is drawn in dashed line. The difference between the maximum of the cross section for $J'=9$ and $J'=11$ is of 0.6% and thus a little bit larger. The peak around 20 eV is related to the photodissociation via the first excited electronic state leading to $He^+(1s)+H(1s)$ and is strongly shifted from the maximum of the $J''=0$ case. The mean equilibrium distance for the $J''=10$ state is 1.86 a.u. while it is 1.49 a.u. for $J''=0$. This leads to a very different Franck Condon gap between the ground and first excited states. However, the cross section is only weakly modified in the range probed by the FEL experiment around 38.7 eV [23]. The same tendency is observed for the $v=1$, $J''=0$ example drawn in dotted line in Fig. 2. The effect is discussed again below (see Fig. 3) for the average cross section over an isotropic orientation.

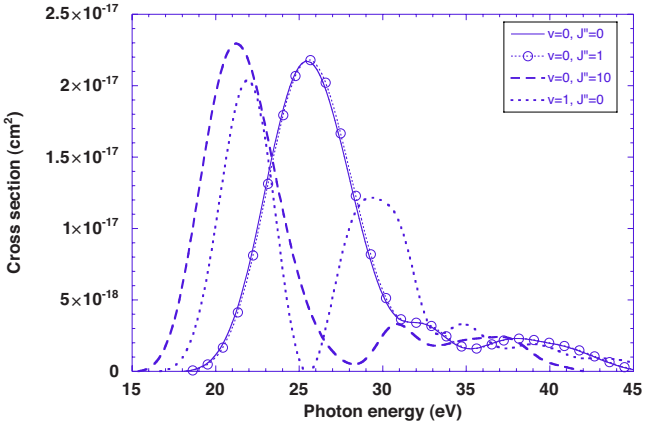

FIG. 2. (Color online) Total photodissociation cross section $\sigma_{0v''J''\to\Lambda'}(E)$ [Eq. (1)] for the transition $^1\Sigma\to{}^1\Sigma$ for the parallel orientation of the molecular axis with respect to the field for the case $J''=0\to J'=1$ (full line), $J''=1\to J'=0,2$ (dotted line with open circles), $J''=10\to J'=9,11$ (dashes) for $v=0$ and $J''=0\to J'=1$ for $v=1$ (dots).

Figure 3 gives the photodissociation cross section for three cases of Fig. 2 averaged over an isotropic orientation by weighting each orientation x, y, z by 1/3. The parallel orientation (μ_z) concerns the transition $^1\Sigma\to{}^1\Sigma$ and the perpendicular orientations (μ_x and μ_y) are related to the $^1\Sigma\to{}^1\Pi$ transitions. One observes that the average cross sections for initial excited rotational and vibrational states are of

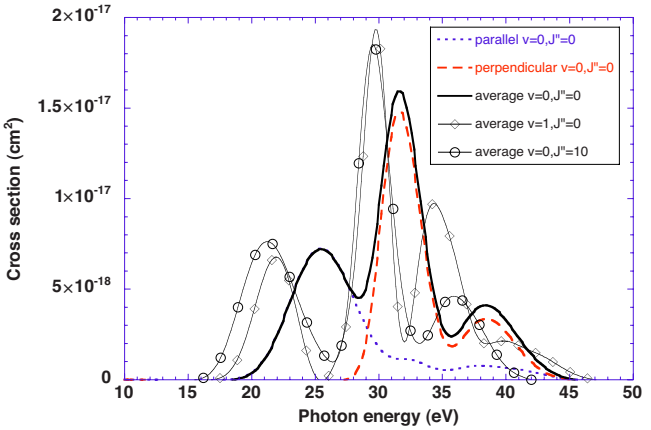

FIG. 3. (Color online) Photodissociation cross section averaged over an isotropic orientation with respect to the laser field, bold line: $J''=0\to J'=1$ for $v=0$ with in dotted line the contribution of the parallel orientation ($^1\Sigma\to{}^1\Sigma$ transitions) and in dashed line, the contribution of the perpendicular orientations ($^1\Sigma\to{}^1\Pi$ transitions); open circles: $J''=10\to J'=9,11$ for $v=0$; diamonds: $J''=0\to J'=1$ for $v=1$.

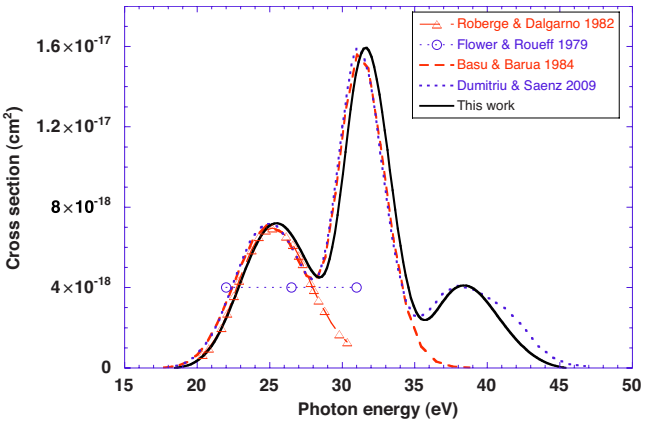

FIG. 4. (Color online) Comparison of the total photodissociation cross section for a isotropic orientation of the molecular axis with respect to the field for the case $v=0$, $J''=1\rightarrow J'=0,2$ with previous works.

the same order of magnitude in the range of 38.7 eV but lower than the value for the $v=0$, $J''=0$ case. The cross section decreases with v in this range (4.1×10^{-18} cm^2 for $v=0$, 2.0×10^{-18} cm^2 for $v=1$ and 2.1×10^{-18} cm^2 for $v=4$). Finally, one observes that the rotational couplings are negligible for $J''=0$ but begin to give some effect for $J''=10$. We have compared the results with and without the rotational couplings for $J''=10$. The cross section for parallel transitions differs by 0.2% but that for perpendicular transitions differs by 3%.

A comparison with previous theoretical works of the total cross section from the state $v=0$, $J''=1$, averaged over an isotropic orientation, is given in Fig. 4. Flower and Roueff [22] consider the ground state and the first excited Σ state. They use the potential energy curves and the dipole moment from Green *et al.* [8] and calculate only one point which they estimate valid in an energy range of 22–31 eV. Roberge and Dalgarno [17] use the curves from Kolos and Peek [9] and the dipole matrix element from Green *et al.* [8] Basu and Barua [11] include a third Σ state as well as the first Π state in their calculation. The agreement with our work is good until about 35 eV, where the contribution from higher excited states becomes dominant. Dumitriu and Saenz [16] recently calculated the cross section. At energies lower than 38 eV, our result is shifted to a larger energy by about 0.55 eV. This shift is probably due to the value of the asymptote of the ground state in Ref. [16] [−78.3 eV ± 0.1 eV from Fig. 1 of Ref. [16] while it is −78.9 eV (−2.898 h) in this work and the experimental value is −79.0 eV (−2.903 h)]. Above 40 eV, our cross section decreases faster, which is due to the fact that we include only states up to $n=3$ in our calculations.

Figure 5(a) shows the partial cross sections computed by Eq. (3) for the fragmentations leading to a section larger than 10^{-18} cm^2. Figure 5(b) gives a zoom of Fig. 5(a) with sections larger than 5×10^{-19} cm^2. For an energy below 32 eV, the dissociation is mainly due to the H($n=1$) channel and the region from 32 to 37 eV is dominated by the fragmentation into He($1s2s$) (open circles) and H($n=2$) (dashed line). We have verified that the two methods based on an asymptotic analysis [Eq. (3) (crosses) and Eq. (4) (diamonds)] give the

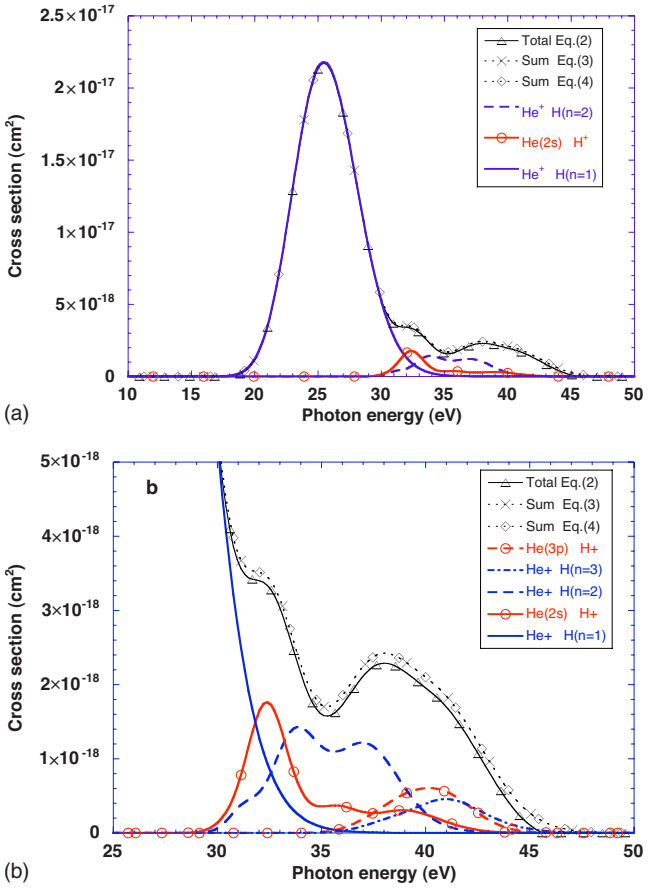

FIG. 5. (Color online) Partial cross sections section computed from Eq. (3) for a parallel orientation for transitions $J''=0\rightarrow J'=1$ from the vibrational state $v=0$. The sum of the partial cross sections is compared with that obtained by Eq. (4) and with the total cross section calculated by Eq. (2). Panel a: sections larger than 10^{-18} cm^2. Panel b: sections larger than 5×10^{-19} cm^2.

same partial cross sections and that their sum converges toward the result obtained by autocorrelation of the promoted state. As shown in the zoom in Fig. 5(b), the discrepancy between the total cross section [Eqs. (1) and (2)] and the sum of the partial cross section is less than 10%.

The partial cross sections obtained in the Born-Oppenheimer approximation by propagating the wave packets on the uncoupled adiabatic states are displayed in Fig. 6. The total cross section is the same as expected but the nonadiabatic couplings modify the distribution of the fragments, particularly the yield of He($1s2s$) and H($n=2$) in the range around 35 eV.

The effect is more spectacular for the dissociation in the Π states of the $n=2$ shell by the perpendicular excitation as shown in Figs. 7(a) and 7(b) showing the partial cross sections in the BO approximation and in the coupled case. The promoted state mainly populates the lower state in this $n=2$ shell which dissociates into He^+ and H($2p$) fragment. The nonadiabatic coupling around $R=10.15$ bohr leads to a charge exchange and a notable redistribution of the He($1s2p$) and H($2p$) fragments [see Fig. 7(b)].

The experimental observations at 32 nm estimate a partial cross section for the fragmentation into H^+ and neutral He

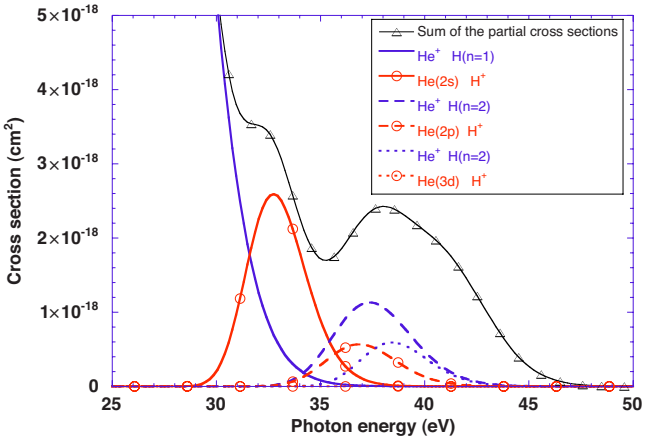

FIG. 6. (Color online) Partial cross sections larger than 5×10^{-19} cm^2 computed from Eq. (3) in the Born-Oppenheimer approximation for a parallel orientation for transitions $J''=0\rightarrow J'=1$ from the vibrational state $v=0$. The sum of the partial cross sections BO (full line) is compared with that the results obtained in the nonadiabatic case (triangles).

equal to $(1.4\pm0.7)\times10^{-18}$ cm^2. In Fig. 8, we sum all the partial sections for channels H^++He($1snl$) with $n\geq2$ and give the average over isotropic distribution. Figure 8(a) presents the BO approach and Fig. 8(b) gives the results obtained with the coupled channels. The BO profile is similar to the simulation of Ref. [16] with a lower maximum value near 40 eV for the contribution of the Π states. The coupled-channel profile is very different, particularly due to the peak in between 32 and 33 eV which comes from the fragmentation into He($1s2p$) from the perpendicular orientation [see Fig. 7(b)]. The peak at 39 eV has a maximum of 3.14×10^{-18} cm^2 and the value at the experimental wavelength is 2.07×10^{-18} cm^2, thus it belongs to the uncertainty bar of the experimental data ($1.4\pm0.7\times10^{-18}$ cm^2). In conclusion, our BO simulation does not agree with the experimental value but the result of the nonadiabatic coupled equations gives good agreement. Furthermore, the simulation confirms that the major part of the fragmentation arise from the excited Π states. This is proven again below by the simulation of the photodissociation with a femtosecond laser pulse.

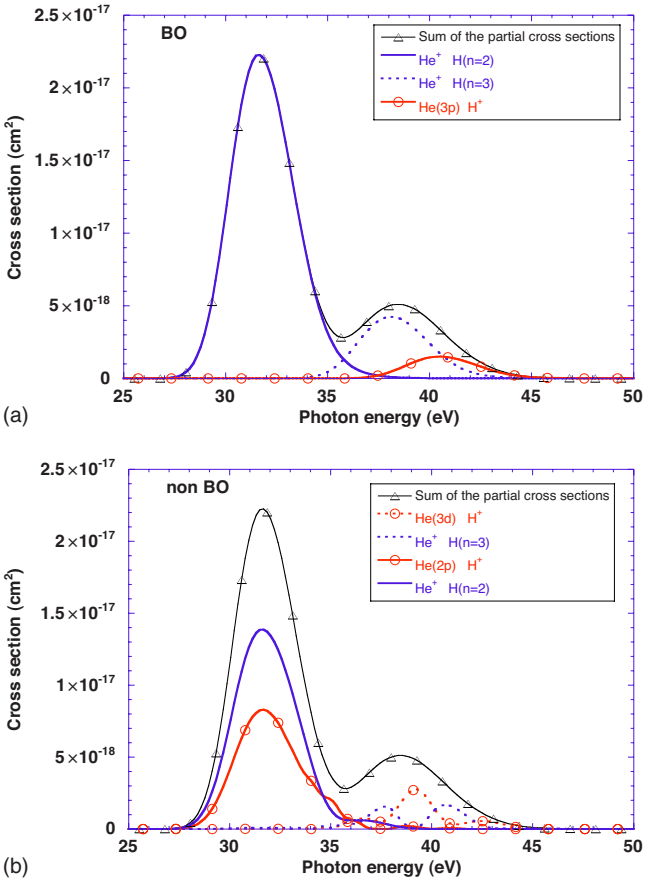

FIG. 7. (Color online) Partial cross sections larger than 10^{-18} cm^2 computed from Eq. (3) for a perpendicular orientation for transitions $J''=0\rightarrow J'=1$ from the vibrational state $v=0$. Panel a: Born-Oppenheimer approximation; panel b: nonadiabatic case.

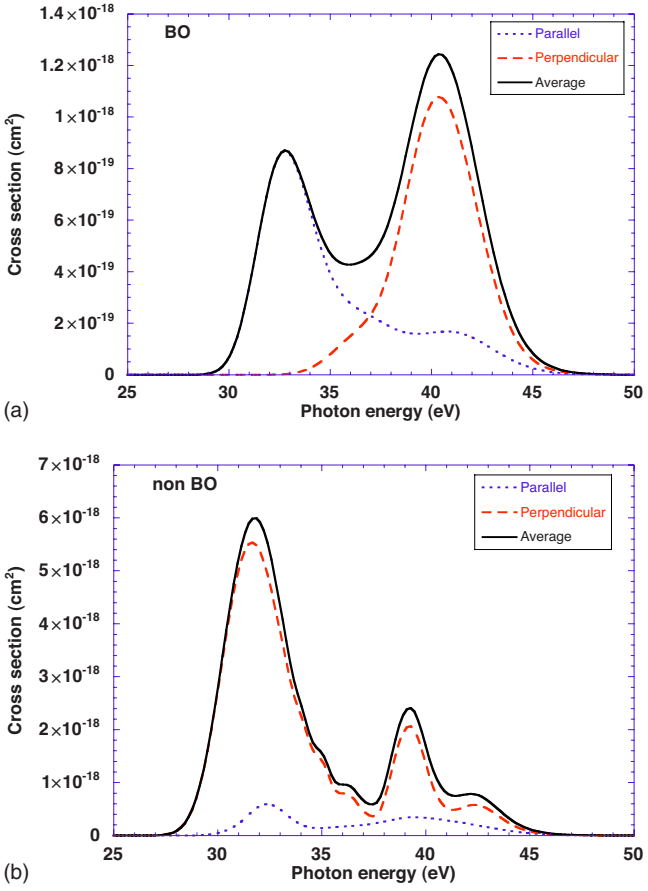

FIG. 8. (Color online) Average partial cross section for the fragmentation into H^+ and neutral He computed from Eq. (3) for an isotropic orientation for transitions $J''=0\rightarrow J'=1$ from the vibrational state $v=0$. Panel a: Born-Oppenheimer approximation; panel b: nonadiabatic case.

IV. SIMULATION WITH A FEMTOSECOND LASER PULSE

The FEL experiment analyzes the neutral He($1snl$) fragment by resolving the kinetic energy release distribution and

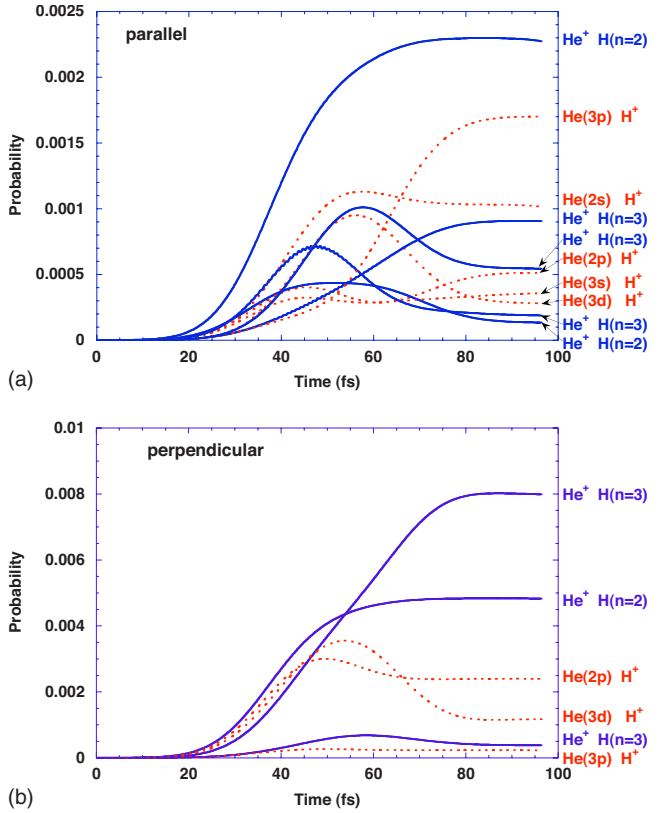

FIG. 9. (Color online) Population in the excited electronic states during the photodissociation of the ground $v=0$, $J=0$ state by a pulse of 30 fs and a maximum intensity of 8.775×10^{11} W cm^{-2}. Panel (a) parallel orientation (Only fragments having an asymptotic probability larger than 3×10^{-4} are shown); panel (b) perpendicular orientation.

the dissociation angle distribution relative to the FEL polarization which is directed along the ion beam. The FEL consists of a sequence of short pulses of about 30 fs separated by 10 μs. The accumulation time to get the photo fragment image is very long of about 13 h [23]. We simulate the impact of a single laser shot of 30 fs and an intensity which is probably larger than the experimental one but leading to transition probabilities of the order of 10^{-3}. The initial state is the $v=0$ $J=0$ state of the ground electronic state. Figure 9 gives an example of time-dependent occupancies of the electronic states [Eq. (5)] during the photodissociation for parallel (Σ states) and perpendicular (Π states) orientations. Only fragments having an asymptotic probability larger than 3×10^{-4} are shown. One observes a larger probability of populating states dissociating into H fragment and a larger probability to obtain He fragment from the Π states than from the Σ states in agreement with the experimental results.

We have computed the kinetic energy release distribution of the fragment He($1snl$) by Fourier transforming the wave packet in the asymptotic region. The distribution averaging over an isotropic orientation is given in Fig. 10. We obtain a large intensity in between 13.5 and 14 eV and a second less intense peak at 16.5 eV. The parallel contribution in the range 13.5 and 14 eV is due to He($1s3s$) and He($1s3p$) and that at 16.5 eV to He($1s2s$). The large perpendicular contribution at 13.5 eV is mainly due to He($1s3p$). The simulation

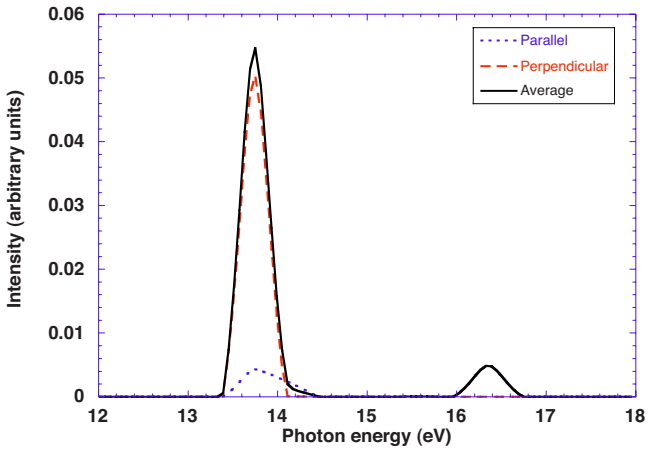

FIG. 10. (Color online) Kinetic energy release for the fragment He($1snl$) during the photodissociation of the ground $v=0$, $J=0$ state by a pulse of 30 fs. The distribution is averaged over an isotropic orientation.

confirms that the major part arises from the excited Π states.

Finally, we simulate the angular distribution of the He fragment for the peak around 13.5 eV. As discussed in Ref. [23] when the fragmentation is very short (here less than 100 fs) the fragmentation angle is related to the orientation of the molecule at the time of the excitation. The angular distribution is computed by the relation [40], $I(\theta)=I_0[1+\beta P_2(\cos\theta)]/4\pi$ with $P_2(\cos\theta)=[3\cos^2\theta-1]/2$. We take for I_0 the maximum value of the peak at 13.8 eV in Fig. 10 for the parallel ($\beta=2$) and the perpendicular ($\beta=-1$) orientation, respectively. The distribution is given in Fig. 11. This result can be compared with the experimental data shown in Fig. 4c of Ref. [23]. However, the latter figure corresponds to a summation over the energy released fragments from 13 to 20 eV including therefore the large contribution at 16.5 eV which is mainly due to an Σ state. This increases the parallel contribution on the experimental graphic when compared with our Fig. 11. Nevertheless, the two figures agree quali-

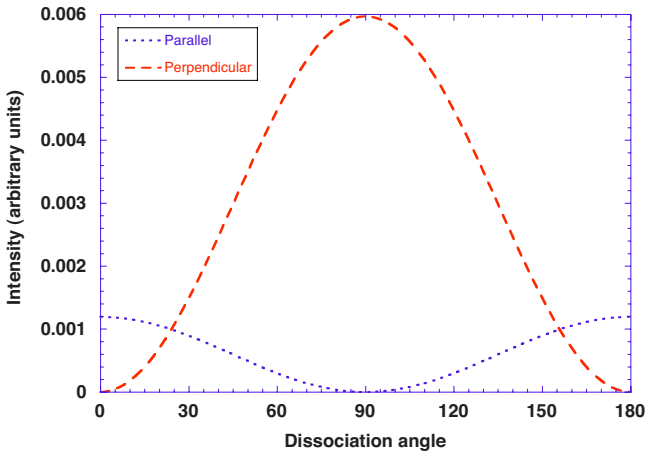

FIG. 11. (Color online) Angular distribution of the He($1snl$) fragment for a kinetic energy release in the range 13.5–14 eV during the photodissociation of the ground $v=0$, $J=0$ state by a pulse of 30 fs. The intensity I_0 is taken from the contribution of the parallel and perpendicular orientation in Fig. 10.

tatively and present a clear dominance of the Π states (perpendicular contribution) over the Σ states (parallel contribution) in both cases.

V. CONCLUSION

We have computed the total and partial photodissociation cross sections of the molecular ion HeH^+ for fragmentation into the excited shells $n=1,2,3$ up to a photon energy of 45 eV. We have analyzed the role of the nonadiabatic interactions and of the rotational couplings. The *ab initio* challenge was to get relevant potential energy curves and nonadiabatic couplings for very excited states. The simulations using the Born-Oppenheimer or diabatic potentials give the same total cross section and are in good agreement with the simulation of Dumitriu *et al.* [16]. However for the partial cross section in a given channel or the branching ratio between H and He fragmentation, we have illustrated that the simulation obtained in the framework of the Born-Oppenheimer model is not sufficient even if it can give accidentally a good agreement with experiment for some energies. The effect of nonadiabatic couplings is more dramatic for perpendicular dissociation via the Π states in the range 30–35 eV, i.e., for dissociation toward $n=1$ and $n=2$ shells. The branching ratio between fragments He or H in the $n=2$ shell cannot be predicted by neglecting the Π states or by neglecting the nonadiabatic couplings.

By considering a highly excited rotational initial state ($J=10$), we have observed that the rotational couplings do not play a significant role and could be neglected for lower rotational quantum numbers for photodissociation. However, rotational excitation could play a significant role because the profile of the total cross section strongly depends of the initial value of J, mainly for dissociation into the $n=1$ shell. Important information for further simulations is the weight of rotationally or vibrationally excited initial states for non-Boltzmann situations.

Furthermore, time-dependent simulations with very accurate methods taking into account couplings among excited states find a renewed interest since the advent of ultrashort laser pulses with energetic photons even for small systems. The time-dependent simulation with a femtosecond Gaussian laser field has provided results which are qualitatively in agreement with the recent FEL laser experiment concerning the order of magnitude of the partial cross section of He neutral fragment at 32 nm and the distribution of the kinetic energy release. We have confirmed the experimental observation that dissociation through Π states dominates the process in the probed energy range.

ACKNOWLEDGMENTS

We thank Dr. B. Lavorel for a helpful discussion. The computing facilities of IDRIS (Projects No. 061247 and No. 2006 0811429) as well the financial support of the FNRS in the University of Liège SUN Nic2 project are gratefully acknowledged. We thank the support of the COST Action CM0702 CUSPFEL. J.L. and N.V. acknowledge the financial support of the Fond National de le Recherche Scientifique (IISN projects) as well as the "Action de Recherche Concertée" ATMOS. K.S. would like to thank The University of Paris-Sud 11 for financial support Grant No. 2238. J.L. thanks the FRIA for financial support.

[1] T. R. Hogness and E. C. Lunn, Phys. Rev. **26**, 44 (1925).
[2] Z. Liu and P. B. Davis, J. Chem. Phys. **107**, 337 (1997).
[3] W. J. van der Zande, W. Koot, D. P. de Bruijn, and C. Kubach, Phys. Rev. Lett. **57**, 1219 (1986).
[4] D. Strasser, K. G. Bhushan, H. B. Pedersen, R. Wester, O. Heber, A. Lafosse, M. L. Rappaport, N. Altstein, and D. Zajfman, Phys. Rev. A **61**, 060705 (2000).
[5] F. B. Yousif, J. B. A. Mitchell, M. Rogelstad, A. Le Paddelec, A. Canosa, and M. I. Chibisov, Phys. Rev. A **49**, 4610 (1994).
[6] Y. Susuki, T. Ito, K. Kimura, and M. Mannami, Phys. Rev. A **51**, 528 (1995).
[7] H. H. Michels, J. Chem. Phys. **44**, 3834 (1966).
[8] T. A. Green, H. H. Michels, J. C. Browne, and M. M. Madsen, J. Chem. Phys. **61**, 5186 (1974); A. Green, H. H. Michels, and J. C. Browne, *ibid.* **64**, 3951 (1976); **69**, 101 (1978).
[9] W. Kolos and J. M. Peek, Chem. Phys. **12**, 381 (1976).
[10] S. Saha, K. K. Datta, and A. K. Barua, J. Phys. B **11**, 3349 (1978).
[11] D. Basu and A. K. Barua, J. Phys. B **17**, 1537 (1984).
[12] A. Saenz, Phys. Rev. A **67**, 033409 (2003).
[13] M. Pavanello, S. Bubin, M. Molski, and L. Adamowicz, J. Chem. Phys. **123**, 104306 (2005).
[14] B.-L. Zhou, J.-M. Zhu, and Z.-C. Yan, Phys. Rev. A **73**, 064503 (2006).
[15] J. Fernández and F. Martin, J. Phys. B **40**, 2471 (2007).
[16] I. Dumitriu and A. Saenz, J. Phys. B **42**, 165101 (2009).
[17] W. Roberge and A. Dalgarno, Astrophys. J. **255**, 489 (1982).
[18] S. Lepp and J. M. Shull, Astrophys. J. **280**, 465 (1984).
[19] D. Galli and F. Palla, Astron. Astrophys. **335**, 403 (1998).
[20] E. A. Engel, N. Doss, G. J. Harris, and J. Tennyson, Mon. Not. R. Astron. Soc. **357**, 471 (2005).
[21] P. C. Stancil, S. Lepp, and A. Dalgarno, Astrophys. J. **509**, 1 (1998).
[22] D. R. Flower and E. Roueff, Astron. Astrophys. **72**, 361 (1979).
[23] H. B. Pedersen, S. Altevogt, B. Jordon-Thaden, O. Heber, M. L. Rappaport, D. Schwalm, J. Ullrich, D. Zajfman, R. Treusch, N. Guerassimova, M. Martins, J.-T. Hoeft, M. Wellhöfer, and A. Wolf, Phys. Rev. Lett. **98**, 223202 (2007).
[24] M. Shapiro and R. Bersohn, Annu. Rev. Phys. Chem. **33**, 409 (1982).
[25] P. S. Shternin and O. S. Vasyutinskii, J. Chem. Phys. **128**, 194314 (2008) and references herein.
[26] J. M. Brown, J. T. Hougen, K.-P. Huber, J. W. C. Johns, I. Kopp, H. Lefebvre-Brion, A. J. Mere, D. A. Ramsey, J. Rostas, and R. N. Zare, J. Mol. Spectrosc. **55**, 500 (1975).
[27] R. N. Zare, *Angular Momentum* (World Scientific, New York, 1988).

[28] P. J. Knowles and H.-J. Werner, Chem. Phys. Lett. **115**, 259 (1985); H.-J. Werner and P. J. Knowles, J. Chem. Phys. **82**, 5053 (1985).

[29] H.-J. Werner, P. J. Knowles, R. D. Amos, A. Bernhardsson, A. Berning, P. Celani, D. L. Cooper, M. J. O. Deegan, A. J. Dobbyn, F. Eckert, C. Hampel, G. Hetzer, T. Korona, R. Lindh, A. W. Lloyd, S. J. McNicholas, F. R. Manby, W. Meyer, M. E. Mura, A. Nicklass, P. Palmieri, R. Pitzer, G. Rauhut, M. Schütz, H. Stoll, A. J. Stone, R. Tarroni, and T. Thorsteinsson, MOLPRO is a package of *ab initio* programs, Department of Chemistry, University of Birmingham, Birmingham B15 2TT, UK.

[30] R. A. Kendall, T. H. Dunning, Jr., and R. J. Harrison, J. Chem. Phys. **96**, 6796 (1992); D. E. Woon and T. H. Dunning Jr., *ibid.* **98**, 1358 (1993).

[31] J. Loreau, P. Palmeri, P. Quinet, J. Liévin, and N. Vaeck (unpublished).

[32] C. Zhu and H. Nakamura, J. Chem. Phys. **106**, 2599 (1997).

[33] A. Hansson and J. K. G. Watson, J. Mol. Spectrosc. **233**, 169 (2005).

[34] E. J. Heller, J. Chem. Phys. **68**, 3891 (1978); **68**, 2066 (1978).

[35] D. J. Tannor, *Introduction to Quantum Mechanics A Time-dependent Perspective* (University Science Books, Sausalito, California, 2007).

[36] G. G. Balint-Kurti, R. N. Dixon, and C. C. Marston, J. Chem. Soc., Faraday Trans. **86**, 1741 (1990).

[37] K. C. Kulander and E. J. Heller, J. Chem. Phys. **69**, 2439 (1978).

[38] M. D. Feit, J. A. Fleck, and A. Steiger, J. Comput. Phys. **47**, 412 (1982); M. D. Feit and J. A. Fleck, J. Chem. Phys. **78**, 301 (1983).

[39] J. Alvarellos and H. Metiu, J. Chem. Phys. **88**, 4957 (1988).

[40] R. N. Zare, Mol. Photochem. **4**, 1 (1972).